Signal Integrity in Pulse-train Excited Array Antennas in Time and Space - A Full TD Analysis

de Hoop, Adrianus T.; Lager, Ion E.

Publication date
2015

Document Version
Accepted author manuscript

Published in
Proceedings of the 9th European Conference on Antennas and Propagation, EuCAP 2015

Citation (APA)
de Hoop, A. T., & Lager, I. E. (2015). Signal Integrity in Pulse-train Excited Array Antennas in Time and Space - A Full TD Analysis. In L. M. Correia (Ed.), *Proceedings of the 9th European Conference on Antennas and Propagation, EuCAP 2015* (pp. 1-5). IEEE.

Important note
To cite this publication, please use the final published version (if applicable).
Please check the document version above.

Signal Integrity in Pulse-train Excited Array Antennas in Time and Space – A Full TD Analysis

Adrianus T. de Hoop and Ioan E. Lager
Delft University of Technology, Faculty of Electrical Engineering, Mathematics and Computer Science,
Mekelweg 4, 2628 CD Delft, the Netherlands, Email: a.t.dehoop@tudelft.nl, i.e.lager@tudelft.nl

***Abstract*—Signal integrity in the far-field radiation from pulse-train excited array antennas is studied via full time-domain instruments. The disturbance in the received signal is related to the fidelity factor. At any point in our analysis, the disturbance is evaluated based on a reduced, well defined set of parameters: pulse parameters and pulse repetition rate – temporal dependence, and elementary radiator location – spatial dependence. Their effect is examined by means of illustrative numerical experiments. These results are expedient for enhancing the detectability of the signals radiated by pulse-train excited array antennas, as needed in wireless digital transfer.**

I. Introduction

Signal integrity is the cornerstone to the error-free recovering of the received binary values in wireless digital transfer [1]. Ensuring this feature in the ultra-high data-rate communication systems that are currently developed [2] becomes increasingly difficult and demands increasingly sophisticated design procedures. A conditional aspect for the successful application of these procedures is the accurate characterisation of the received signals. To this end, electromagnetic (EM) models can opportunely predict the system performance under certain simple, but relevant conditions. Since (ultra-high rate) digital signal transfer is best supported by *pulsed* electromagnetic (EM) field transfer, such models are most adequately built by means of time-domain (TD) instruments.

Wireless digital transmitting and receiving *trains* of *pulses*. All pulses in EM models should have analytical expressions that, moreover, should characterised by generally accepted parameters such pulse amplitude, pulse rise time, pulse time width, pulse fall time [3], [4]. Furthermore, the (coded) pulses are sent at regular intervals, this inducing a pulse repetition rate. These pulse-trains undergo alterations during the transmitter $\rightarrow$ receiver transfer:

1) Temporal dependence: For a receiver to be located in the far-field region [5, pp. 762–768], the received EM field is the time-derivative of the electric current that excites the Kirchhoff port of the emitter. Furthermore, depending on the pulse repetition rate, pulses can partially overlap the tail of the preceding ones, this further deteriorates the information content in the signal. Such effects constitute the received signal's *temporal dependence* on the exciting current and manifest themselves even for isolated elements.

2) Spatial dependence: For increasing the energy of the received signals and, thus, improving their detection in background noise, wireless systems often resort to energy focussing by means of array antennas on the transmit and/or receive side. The conjunction of elements' locations and time delays of the feeding signals yields constructive/destructive interference in different directions (see the TD study in [6]). Additionally, the element spreading results into different path lengths for the elementary signals that, in turn, may yield additional pulse overlapping, with both possible deleterious effects (further deterioration of the signal integrity in desired directions) and possible beneficial effects (drastic disturbance of the received signal in other directions – favourable for security purposes). The element spreading induced pulse overlapping constitutes the received signal's *spatial dependence* on the exciting current and is specific to array configurations.

In this paper we examine the signal integrity's spatial dependence in the case of pulse-train excited array antennas. To this end, we opt for an analytic TD modelling of the EM field, the excitation being taken as short trains of monocycle pulses [3]. The radiated field signatures are used for evaluating the *system's fidelity factor*, [7] a widely employed quantitative measure to characterise the performance of high-speed digital data transmission. As has been demonstrated in [7], this fidelity factor is composed out of the *signal fidelity factors* of the constituting subsystems in the relevant transmission chain. From this perspective, we analyse the *directional signal fidelity factor* that also accounts for the array antenna's beam-steering properties. The resulting signal fidelity factor is a purely directional quantity.

Our study starts by recapitulating the results in [6] concerning the TD far-field EM radiation from arbitrary array antennas. These results will be then employed for examining this radiation in the case of isolated radiators and linear arrays. Our account will end with conclusions.

II. Radiation of array antennas composed of pulsed electric-current excited elements

A. Examined configuration

The antenna is composed of $N+1,\ N=0,1,2\ldots$, identical, mutually translationally shifted, pulsed electric-current excited elements (Fig. 1). Position in the examined configuration is specified by the position vector $\boldsymbol{x}\in\mathbb{R}^3$ and the time coordinate is $t\in\mathbb{R}$.

Let $\mathcal{D}_0$ denote the spatial support of the reference element and let $\chi_0(\boldsymbol{x})$ be its characteristic set, i.e., $\chi_0(\boldsymbol{x})=\{0,1/2,1\}$ for $\boldsymbol{x}\in\{\mathcal{D}_0,\partial\mathcal{D}_0,\mathcal{D}_0^\infty\}$, where $\partial\mathcal{D}_0$ is the piecewise smooth boundary of $\mathcal{D}_0$ and $\mathcal{D}_0^\infty$ is the (unbounded) complement of $\mathcal{D}_0\cup\partial\mathcal{D}_0$ in $\mathbb{R}^3$. The spatial support $\mathcal{D}_n$ of the by $\boldsymbol{r}_n$ with respect to $\mathcal{D}_0$ translationally shifted element has the characteristic set $\chi_n(\boldsymbol{x})=\chi_0(\boldsymbol{x}+\boldsymbol{r}_n)$. The support of the

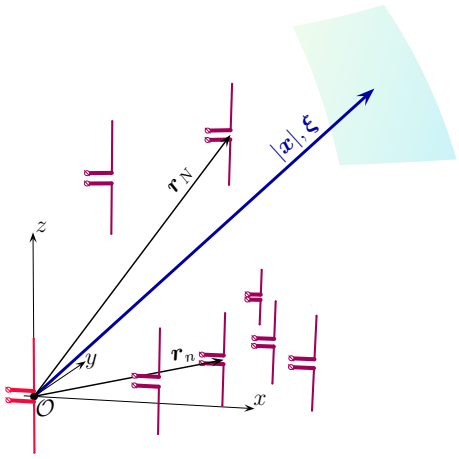

Fig. 1. Antenna array composed of identical, translationally shifted elements.

entire array is then

$$\mathcal{D} = \bigcup_{n=0}^{N} \mathcal{D}_n. \tag{1}$$

The elements carry electric currents with volume density $\boldsymbol{J}(\boldsymbol{x},t)$. Each element of is accessible via a one-port Kirchhoff circuit that is available for excitation. The volume densities of electric current in $\mathcal{D}_n$ are $\boldsymbol{J}_n^{\delta}(\boldsymbol{x},t)$ in case its Kirchhoff circuit port is excited with a Dirac delta pulse $\delta(t)$ and

$$\boldsymbol{J}_n(\boldsymbol{x},t) = I_n^{\mathrm{G}}(t) \overset{(t)}{*} \boldsymbol{J}_n^{\delta}(\boldsymbol{x},t) \tag{2}$$

in case its Kirchhoff circuit port is excited with the electric current $I_n^{\mathrm{G}}(t)$, with $\overset{(t)}{*}$ denoting time convolution. By neglecting mutual coupling, it then follows that

$$\boldsymbol{J}_n^{\delta}(\boldsymbol{x},t) = \boldsymbol{J}_0^{\delta}(\boldsymbol{x}+\boldsymbol{r}_n,t), \quad \text{for } n = 1,\ldots,N. \tag{3}$$

The array radiates into free space, withelectric permittivity ε_0, magnetic permeability μ_0 and corresponding wavespeed $c_0 = (\varepsilon_0\mu_0)^{-1/2}$.

B. The radiated field

The radiated field is expressed in terms of the electric-current potential $\boldsymbol{A}(\boldsymbol{x},t)$ that satisfies the vector wave equation

$$(\boldsymbol{\nabla}\cdot\boldsymbol{\nabla})\,\boldsymbol{A} - c_0^{-2}\partial_t^2\boldsymbol{A} = -\boldsymbol{J} \tag{4}$$

with

$$\boldsymbol{J}(\boldsymbol{x},t) = \sum_{n=0}^{N} \boldsymbol{J}_n(\boldsymbol{x},t)\chi_n(\boldsymbol{x},t) \tag{5}$$

being the volume density of electric current in $\mathcal{D}$. With

$$G(\boldsymbol{x},t) = \frac{\delta(t-|\boldsymbol{x}|/c_0)}{4\pi|\boldsymbol{x}|} \quad \text{for } \boldsymbol{x} \neq \boldsymbol{0} \tag{6}$$

as the Green's function of the scalar wave equation

$$(\boldsymbol{\nabla}\cdot\boldsymbol{\nabla})\,G - c_0^{-2}\partial_t^2 G = -\delta(\boldsymbol{x},t) \tag{7}$$

it follows that

$$\boldsymbol{A}(\boldsymbol{x},t) = \sum_{n=0}^{N} \boldsymbol{A}_n(\boldsymbol{x},t) \tag{8}$$

with

$$\boldsymbol{A}_n(\boldsymbol{x},t) = G(\boldsymbol{x},t) \overset{(\boldsymbol{x})(t)}{*\,*} \boldsymbol{J}_n(\boldsymbol{x},t) \;\text{ for } \boldsymbol{x} \in \mathbb{R}^3, \tag{9}$$

in which $\overset{(\boldsymbol{x})}{*}$ denotes spatial convolution (which, in this case, is extended over $\mathcal{D}$). From Maxwell's equations, the corresponding electric and magnetic field strengths are [5, Eqs. (26.3-1) and (26.3-2)]

$$\boldsymbol{E} = -\mu_0\partial_t\boldsymbol{A} + \epsilon_0^{-1}\mathbf{l}_t\boldsymbol{\nabla}(\boldsymbol{\nabla}\cdot\boldsymbol{A}) \tag{10}$$

$$\boldsymbol{H} = \boldsymbol{\nabla}\times\boldsymbol{A}, \tag{11}$$

where $\mathbf{l}_t$ denotes the time integration operator defined as

$$\mathbf{l}_t[f(\boldsymbol{x},t)] = \int_{\tau=-\infty}^{t} f(\boldsymbol{x},\tau)\mathrm{d}\tau. \tag{12}$$

C. The TD far-field radiation characteristics

Let the TD far-field expression

$$\{\boldsymbol{A},\boldsymbol{E},\boldsymbol{H}\}(\boldsymbol{x},t) = \frac{\{\boldsymbol{A}^{\infty},\boldsymbol{E}^{\infty},\boldsymbol{H}^{\infty}\}(\boldsymbol{\xi},t-|\boldsymbol{x}|c_0^{-1})}{4\pi|\boldsymbol{x}|}\left[1+O(|\boldsymbol{x}|^{-1})\right] \quad \text{as } |\boldsymbol{x}|\to\infty \tag{13}$$

with $\mathcal{O}$ as the reference center and $\boldsymbol{\xi} = \boldsymbol{x}/|\boldsymbol{x}|$ as the unit vector in the direction of observation. The far-field radiation characteristics $\{\boldsymbol{A}^{\infty},\boldsymbol{E}^{\infty},\boldsymbol{H}^{\infty}\}(\boldsymbol{\xi},t)$ are interrelated by [5, Eqs. (26.3-13) and (26.3-16)]

$$\boldsymbol{E}^{\infty} = -\mu_0[\partial_t\boldsymbol{A}^{\infty} - \boldsymbol{\xi}(\boldsymbol{\xi}\cdot\partial_t\boldsymbol{A}^{\infty})] \tag{14}$$

$$\boldsymbol{H}^{\infty} = -c_0^{-1}\boldsymbol{\xi}\times\partial_t\boldsymbol{A}^{\infty}. \tag{15}$$

D. Beam shaping and beam steering

For a given positioning of the elements in the array, the standard practice for its beam steering is to select a reference pulse $I_0^{\mathrm{G}}(t)$ for exciting $\mathcal{D}_0$ and taking $\{I_n^{\mathrm{G}}(t); n = 1,2,3,\ldots,N\}$ to be time-shifted versions of it $I_n^{\mathrm{G}}(t) = I_0^{\mathrm{G}}(t-T_n)$, with T_n the relevant time delays. With (2) and (3), it then follows that

$$\boldsymbol{A}^{\infty} = \sum_{n=0}^{N} \boldsymbol{A}_n^{\infty}, \tag{16}$$

in which

$$\boldsymbol{A}_n^{\infty} = I_0^{\mathrm{G}}(t-T_n) \overset{(t)}{*} \int_{\mathcal{D}_n} \boldsymbol{J}_0^{\delta}[\boldsymbol{x}',t+c_0^{-1}\boldsymbol{\xi}\cdot(\boldsymbol{x}'+\boldsymbol{r}_n)]\mathrm{d}V(\boldsymbol{x}'). \tag{17}$$

By rewriting this time convolution, it follows that constructive interference of the element contributions occurs if

$$T_n = c_0^{-1}\boldsymbol{\xi}_{\mathrm{st}}\cdot\boldsymbol{r}_n, \quad \text{for } n = 1,2,3,\ldots,N. \tag{18}$$

The resulting $\boldsymbol{\xi}_{\mathrm{st}}$ specifies the direction of the main beam ('direction of steering').

E. The area density of radiated energy

The energy W^{rad} radiated by the array is expressed as

$$W^{\mathrm{rad}} = \int_{\boldsymbol{\xi}\cdot\boldsymbol{\xi}=1} \boldsymbol{\Phi}^{\mathrm{rad}}(\boldsymbol{\xi})\cdot\boldsymbol{\xi}\,\mathrm{d}\Omega, \tag{19}$$

in which $\boldsymbol{\Phi}^{\mathrm{rad}}(\boldsymbol{\xi})$ is the area density of radiated energy in the direction $\boldsymbol{\xi}$. For free space radiation, it is found that [6]

$$\boldsymbol{\Phi}^{\mathrm{rad}}(\boldsymbol{\xi}) = \frac{Z_0}{16\pi^2\, c_0^2}\,\boldsymbol{\xi}\int_{t\in\mathbb{R}} \left[\partial_t\left(\boldsymbol{\xi}\times\boldsymbol{A}^{\infty}\right)\cdot\partial_t\left(\boldsymbol{\xi}\times\boldsymbol{A}^{\infty}\right)\right]\mathrm{d}t \tag{20}$$

with $Z_0 = (\mu_{/\varepsilon_0})^{½}$ denoting the free space electromagnetic wave impedance.

III. Illustrative Numerical Experiments

The overall quality of an antenna is given by the directional distribution of radiated energy and the signal fidelity as it contributes to the overall system fidelity factor. In this section, the directional distribution of radiated energy and the signal integrity in pulse-train excited array antennas is analysed by examining the quantities defined in Section III-C.

A. Excitation electric current shapes

The shapes of the electric current $I_n^{\mathrm{G}}(t)$ exciting the Kirchhoff circuit ports of the array elements are taken as short trains of monocycle (d_tPE) pulses. Their expression follows from the normalised power exponential (PE) pulse [3] of pulse rise time $t_{\mathrm{r}} > 0$ and pulse rising power $\nu > 1$ (with ν being confined to integer values in this study) as

$$\begin{aligned}\mathrm{d}_t\mathrm{PE}(t) &= N(\nu)\,\partial_t\mathrm{PE}(t)\\ &= N(\nu)\left(t'^{\nu-1} - t'^{\nu}\right)\exp\left[-\nu\left(t'-1\right)\right]H(t)\end{aligned} \tag{21}$$

where $t' = t/t_{\mathrm{r}}$,

$$N(\nu) = \frac{t_{\mathrm{r}}}{\nu^{½}}\left(\frac{\nu^{½}}{\nu^{½}-1}\right)^{\nu-1}\exp(-\nu^{½}) \tag{22}$$

ensures a unit amplitude for d_tPE and $H(\cdot)$ is the Heaviside unit step function. Since $\mathrm{d}_t\mathrm{PE}(t_{\mathrm{r}}) = 0$, t_{r} is also denoted in the case of d_tPE as the zero-crossing time $t_{0\mathrm{x}}$. In line with [3, Eq. (23)], the pulse time width t_{w} is

$$t_{\mathrm{w}} = \int_0^{t_{\mathrm{r}}} \mathrm{d}_t\mathrm{PE}(t)\,\mathrm{d}t = N(\nu)\int_0^{t_{\mathrm{r}}} \partial_t\mathrm{PE}(t)\,\mathrm{d}t = N(\nu). \tag{23}$$

The electric current injected at the Kirchhoff port of the reference element in the array is then taken as

$$I_{\mathrm{ref}}^{\mathrm{G}}(t) = \sum_{m=0}^{M} I_0\ \mathrm{d}_t\mathrm{PE}(t + mR_{\mathrm{r}}) \tag{24}$$

in which I_0 is the electric current amplitude and R_{r} the pulse repetition rate, with the current excitations of the remaining elements being time delayed according to (18).

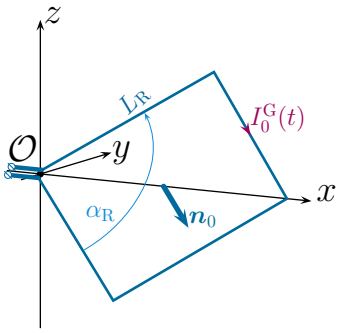

Fig. 2. Rhombic antenna element. Its geometric parameters are the opening angle α_{R} and the side length L_{R}. The reference element is represented; its orientations are taken as $\boldsymbol{n}_0\cdot\boldsymbol{i}_z = 0$ or $\boldsymbol{n}_0\cdot\boldsymbol{i}_z = 1$.

B. Examined configurations

The array antennas are taken in this paper to consist of rhombic wire antennas (see Fig. 2). In all experiments, $\alpha_{\mathrm{R}} = 90°$ and $L_{\mathrm{R}} = c_0 t_{\mathrm{w}}/20$. Our investigations will concern isolated elements and uniform, linear arrays, the location of the elements being taken as $\boldsymbol{r}_n \parallel \boldsymbol{i}_z$. As indicated in the Introduction, the elements in the array are identical, mutually translationally shifted. The reference element $(n = 0)$ is taken to have two possible orientations, i.e., $\boldsymbol{n}_0\cdot\boldsymbol{i}_z = 0$ or $\boldsymbol{n}_0\cdot\boldsymbol{i}_z = 1$.

C. Examined quantities

The main analysis in this paper concerns the system's fidelity factor. To this end, we start from the fidelity factor's expression in [8]

$$F(S_{\mathrm{sys}}, S_{\mathrm{ref}}) = \max_{\tau}\int_{t=-\infty}^{\infty} \frac{S_{\mathrm{sys}}(t)}{\|S_{\mathrm{sys}}(t)\|}\frac{S_{\mathrm{ref}}(t-\tau)}{\|S_{\mathrm{ref}}(t)\|}\mathrm{d}t \tag{25}$$

in which S_{sys} and S_{ref} are *scalar* signals and the maximum of the normalised cross-correlation integral is obtained empirically. Since we aim at examining the fidelity of a *subsystem* of the transmission chain, namely that pertaining to the array configuration, we define the array's *directional signal fidelity factor* as

$$F_{\mathrm{f}}(\boldsymbol{\xi}) = \max_{\tau}\int_{t=-\infty}^{\infty} \frac{\boldsymbol{A}^{\infty}(\boldsymbol{\xi},t)\cdot\boldsymbol{A}_0^{\infty}(\boldsymbol{\xi},t-\tau)}{\|\boldsymbol{A}^{\infty}(\boldsymbol{\xi},t)\|\,\|\boldsymbol{A}_0^{\infty}(\boldsymbol{\xi},t)\|}\mathrm{d}t \tag{26}$$

$\boldsymbol{A}_0^{\infty}(\boldsymbol{\xi},t)$ being the electric-current potential corresponding to the reference element. With these choices, the resulting signal fidelity factor is a purely directional quantity that we term as the *directional signal fidelity factor*

We also examine the area density of radiated energy via polar diagrams of the quantity

$$D_{\mathrm{dB}}(\boldsymbol{\xi}) = 10\log_{10}\left[\boldsymbol{\Phi}^{\mathrm{rad}}(\boldsymbol{\xi})\cdot\boldsymbol{\xi}/4\pi W^{\mathrm{rad}}\right] \tag{27}$$

namely the area density of the radiated energy normalised with respect to the one corresponding to an isotropic radiator.

D. Single element experiments

We start by studying isolated rhombic antennas. The $D_{\mathrm{dB}}(\boldsymbol{\xi})$ pattern (see Fig. 3) has the 'doughnut' shape that is characteristic for dipoles, with the nulls in the direction perpendicular to the rhomb's plane. As expected, $F_{\mathrm{f}}(\boldsymbol{\xi})$ (see

Fig. 4) is one in all directions (except, of course, in the ones corresponding to the radiation nulls).

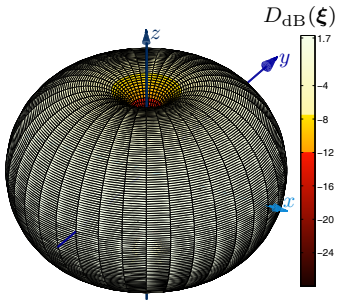

Fig. 3. $D_{\mathrm{dB}}(\boldsymbol{\xi})$ pattern for a rhombic antenna rotated by $\varphi_{\mathrm{R}} = 90°$; excitation: a train of 5 d$_t$PE pulses with a R_{r} pulse repetition rate.

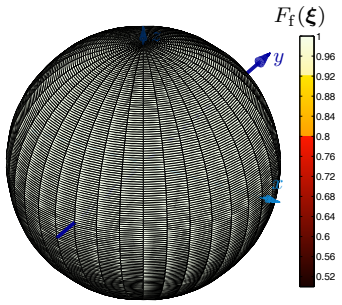

Fig. 4. Fidelity factor pattern for the rhombic antenna examined in Fig. 3.

E. Uniform linear array experiments

We now investigate the case of uniform linear array antennas consisting of 8 elements located at $\boldsymbol{r}_n = z_n \boldsymbol{i}_z$, in which $z_n = n\,(c_0 R_{\mathrm{r}}/2)\,,\ n = 0, 1, 2, \ldots, 7$.

Firstly, we consider the case of broadside scanning. $D_{\mathrm{dB}}(\boldsymbol{\xi})$ patterns are given in Fig. 5. The main beam is clearly visible. As for the sidelobes: (i) The largest ones follow from the superposition of delayed elementary contributions originating from *a part* of the array elements – a phenomenon that was also highlighted in [9]. (ii) There are, also, sidelobes that are not related to correspondences between the pulse repetition rate and element locations, such as the ones pointing in the $\boldsymbol{i}_z$ – direction in Fig. 5.a. Such lobes have also been observed in the patterns reported in [6] for single-pulse excitations. The $F_{\mathrm{f}}(\boldsymbol{\xi})$ patters are shown in Fig. 6. From these plots it is clear that the fidelity factor is, practically, one in the main beam (except in the directions of the radiation nulls) and drops rapidly outside it. We can now conclude that the radiated signal's fidelity significantly increases the spatial selectivity offered by the array's focusing (with an additional gain of at least 3dB). This observation is important for high data-rate transfers, both from the point of view of transfer effectiveness and from that of communication security.

Secondly, we consider the case of the beam being steered at $\widehat{\boldsymbol{\xi}_{\mathrm{st}}, \boldsymbol{i}_z} = 30°$. The $D_{\mathrm{dB}}(\boldsymbol{\xi})$ patterns are given in Fig. 7. The bean scanning is adequately illustrated. As expected, the sidelobes are displaced, with the pertaining observations made for broadside scanning maintaining their validity The $F_{\mathrm{f}}(\boldsymbol{\xi})$ patters are shown in Fig. 8. The unit fidelity factor follows the beam scanning. Note that in the case of the array with

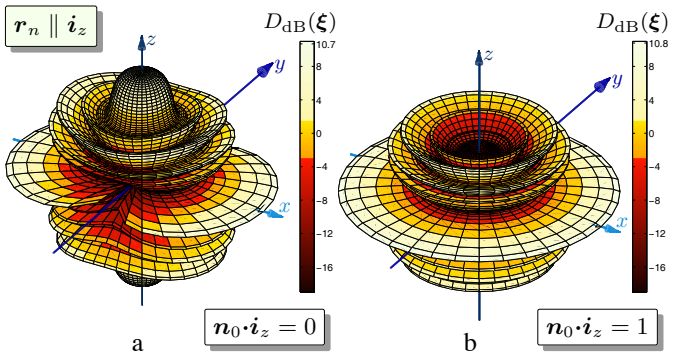

Fig. 5. $D_{\mathrm{dB}}(\boldsymbol{\xi})$ pattern for a uniform, linear array consisting of 8 rhombic antennas; excitation: a train of 5 d$_t$PE pulses with a R_{r} pulse repetition rate; inter-element spacing: $c_0 R_{\mathrm{r}}/2$; broadside beam steering.

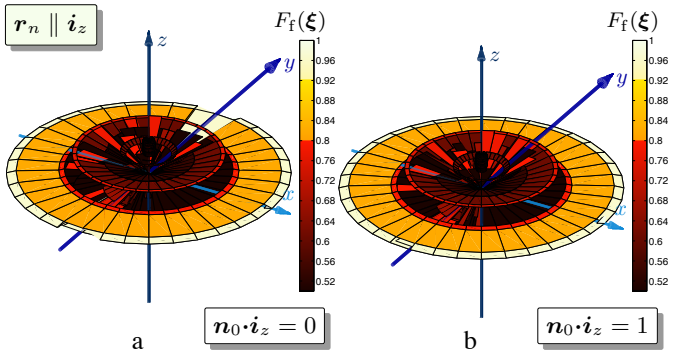

Fig. 6. Fidelity factor pattern for the array examined in Fig. 5.

$\boldsymbol{n}_0 \cdot \boldsymbol{i}_z = 0$ oriented elements, the fact that the beam is steered away from the radiation null results in a unit fidelity factor in the complete main beam. All other observations made for broadside scanning are still applicable.

IV. Conclusions

The signal integrity in the far-field radiation from pulse-train excited array antennas was studied via full time-domain instruments. The directive fidelity factor was employed as a quantitative measure to characterise the disturbance in the radiated EM field. Furthermore, the angular variation of the area density of radiated energy was employed for characterising the spatial dependence of the radiated field levels (the arrays' beam scanning properties). The study demonstrated that the signal's fidelity improves the spatial selectivity offered by the arrays' focusing properties, with an additional 3dB sidelobes reduction being evidenced. This higher spatial selectivity is beneficial for both focusing the EM signals in desired directions, this enhancing the detectability of signals in the inherently signal-to-noise limited receiver units, and for improving the communication security. In this manner, our results are expedient in the field of high data-rate wireless transfer.

Appendix

A. The TD field radiated by array antennas consisting of rhombic elements

For evaluating the TD field radiated by the array antennas considered in this paper, we observe that $\boldsymbol{A}_n^{\infty}$ in (16)

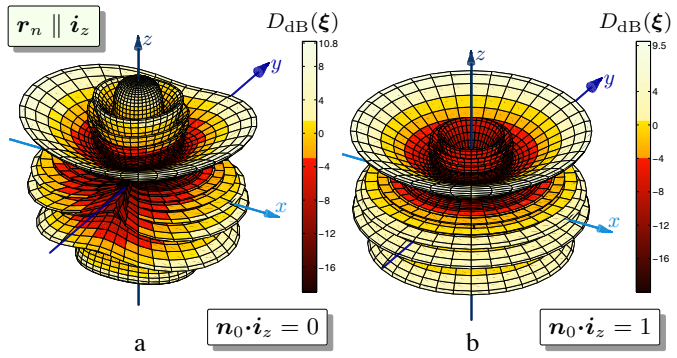

Fig. 7. $D_{\mathrm{dB}}(\boldsymbol{\xi})$ pattern for a uniform, linear array consisting of 8 rhombic antennas; excitation: a train of 5 d_tPE pulses with a R_{r} pulse repetition rate; inter-element spacing: $c_0 R_{\mathrm{r}}/2$; beam steered at $\widehat{\boldsymbol{\xi}_{\mathrm{st}}, \boldsymbol{i}_z} = 30°$.

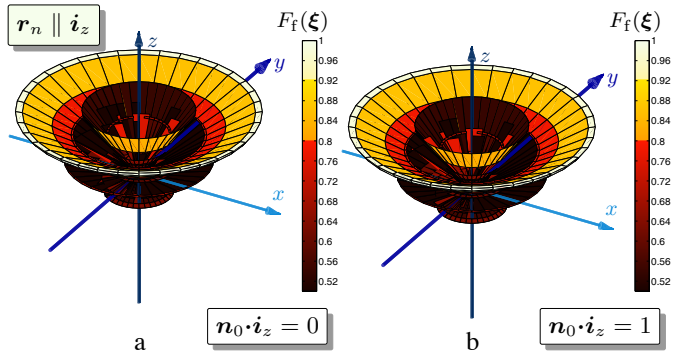

Fig. 8. Fidelity factor pattern for the array examined in Fig. 7.

correspond to fields radiated by straight wire segments of length L_{R}. Let such a segment be oriented from the point with position vector $\boldsymbol{x}_{\mathcal{P}}$ to the point with position vector $\boldsymbol{x}_{\mathcal{Q}}$ (with $\boldsymbol{\tau}_{\mathcal{PQ}} = (\boldsymbol{x}_{\mathcal{Q}} - \boldsymbol{x}_{\mathcal{P}})/L_{\mathrm{R}}$ denoting the unit vector along the tangent to the wire segment) and let $I_n(t)$ be the electric current carried by it. The relevant $\boldsymbol{A}_n^{\infty}$ is then expressed as [6]

$$\partial_t \boldsymbol{A}_{n,\perp}^{\infty}(\boldsymbol{\xi}, t) = (\boldsymbol{\tau}_{\mathcal{PQ}} L_{\mathrm{R}})\, \partial_t I_n(t + c_0^{-1} \boldsymbol{\xi} \cdot \boldsymbol{x}_{\mathcal{P}}) \tag{28}$$

in case $\boldsymbol{\xi} \cdot \boldsymbol{\tau}_{\mathcal{PQ}} = 0$ or as

$$\partial_t \boldsymbol{A}_{n,\not\perp}^{\infty}(\boldsymbol{\xi}, t) = (\boldsymbol{\tau}_{\mathcal{PQ}} L_{\mathrm{R}})\, \frac{I_n\left(t + c_0^{-1} \boldsymbol{\xi} \cdot \boldsymbol{x}_{\mathcal{Q}}\right) - I_n\left(t + c_0^{-1} \boldsymbol{\xi} \cdot \boldsymbol{x}_{\mathcal{P}}\right)}{(\boldsymbol{\xi} \cdot \boldsymbol{\tau}_{\mathcal{PQ}})\, c_0^{-1} L_{\mathrm{R}}} \tag{29}$$

in case $\boldsymbol{\xi} \cdot \boldsymbol{\tau}_{\mathcal{PQ}} \neq 0$. Note that for deriving (28) and (29) it was assumed that $I_n(t)$ has a linear spatial variation along the wire segment, this being consistent with the choice $L_{\mathrm{R}} \ll c_0 t_{\mathrm{w}}$ (see Section III-B).

REFERENCES

[1] J. F. Buckwalter, "Predicting microwave digital signal integrity," *IEEE Trans. Adv. Packag.*, vol. 32, no. 2, pp. 280–289, May 2009.

[2] I. E. Lager, R. B. Staszewski, A. B. Smolders, and D. M. W. Leenaerts, "Ultra-high data-rate wireless transfer in a saturated spectrum – new paradigms," accepted for 44^{th} EuMC, Rome, Italy, Oct. 2014.

[3] I. E. Lager, A. T. de Hoop, and T. Kikkawa, "Model pulses for performance prediction of digital microelectronic systems," *IEEE Trans. Compon., Packag., Manuf. Technol.*, vol. 2, no. 11, pp. 1859–1870, Nov. 2012.

[4] I. E. Lager and A. T. de Hoop, "Causal pulses with rectangular spectral content: A tool for TD analysis of UWB antenna performance," *IEEE Antennas Wireless Propag. Lett.*, vol. 12, no. 1, pp. 1488–1491, Dec. 2013.

[5] A. T. de Hoop, *Handbook of Radiation and Scattering of Waves*, London: Academic Press, 1995, xxx + 1085 pp.; electronic reproduction (with corrections) 2008, freely downloadable, for private use, from http://www.atdehoop.com.

[6] I. E. Lager and A. T. de Hoop, "TD radiation properties of array antennas composed of pulsed electric-current excited elements," *IEEE Antennas Wireless Propag. Lett.*, vol. 15, 2015.

[7] D. Lamensdorf and L. Susman, "Baseband-pulse-antenna techniques," *IEEE Antennas Propag. Mag.*, vol. 36, no. 1, pp. 20–30, Feb. 1994.

[8] E. Pancera, T. Zwick, and W. Wiesbeck, "Spherical fidelity patterns of UWB antennas," *IEEE Trans. Antennas Propag.*, vol. 59, no. 6, pp. 2111–2119, June 2011.

[9] A. Shlivinski, "Kinematic properties of short-pulsed sparse transmitting arrays," *Progress in Electromagnetics Research*, vol. 115, pp. 11–33, 2011, [Online]. doi:10.2528/PIER11020901.